High-dimensional characterization of IL-10 production and IL-10 dependent regulation during primary gammaherpesvirus infection

Abigail K. Kimball[1], Lauren M. Oko[2], Rachael E. Kaspar[1], Linda F. van Dyk[2], and Eric T. Clambey[1]*

[1] Department of Anesthesiology and [2]Department of Immunology and Microbiology, University of Colorado Denver, Anschutz Medical Campus, Aurora, CO 80045

* Address correspondence and reprint requests to Dr. Eric T. Clambey, Department of Anesthesiology, School of Medicine, University of Colorado Anschutz Medical Campus, 12700 E. 19th Ave., Box 112, Aurora, CO, 80045. E-mail address: Eric.Clambey@ucdenver.edu

Running title: CyTOF analysis of IL-10 in gammaherpesvirus infection

ORCIDs: 0000-0002-9831-386X (A.K.K.); 0000-0002-7125-7036 (L.M.O.); 0000-0002-1181-7919 (R.E.K.); 0000-0003-2662-5554 (L.F.v.D.); 0000-0002-7972-9544 (E.T.C.).

This work was funded by National Institutes of Health Grants R01 AI121300 and R01 CA168558 (to L.F.v.D.), an American Heart Association National Scientist Development grant (#13SDG14510023), the Crohn's and Colitis Foundation of America (#311295), a

24 pilot grant from the Lung, Head and Neck Cancer program within the University of
25 Colorado Cancer Center, and a Career Enhancement Award from the University of
26 Colorado Lung Cancer Specialized Program of Research Excellence (P50CA58187) (all
27 to E.T.C.).
28
29 The Lung, Head and Neck program within the University of Colorado Cancer Center,
30 and the Flow Cytometry Shared Resource, are directly funded through support from the
31 National Cancer Institute Cancer Center Support Grant P30CA046934.
32
33 Abbreviations used in this article: B6, C57BL/6; CyTOF, cytometry by time-of-flight;
34 γHV68, murine gammaherpesvirus 68; IFNγ, Interferon-gamma, IL-10, Interleukin-10;
35 ICCS, Intracellular cytokine stain; KO, knockout; TNFα, tumor necrosis factor-alpha,
36 tSNE, t-distributed stochastic neighbor embedding.

ABSTRACT

Interleukin (IL)-10 is a potent immunomodulatory cytokine produced by multiple cell types to restrain immune activation. Many herpesviruses use the IL-10 pathway to facilitate infection, but how endogenous IL-10 is regulated during primary infection in vivo remains poorly characterized. Here, we infected mice with murine gammaherpesvirus 68 (γHV68) and analyzed the production, and genetic contribution, of IL-10 by mass cytometry (cytometry by time-of-flight, CyTOF) analysis. γHV68 infection elicited a breadth of effector CD4 T cells in the lungs of acutely infected mice, including a highly activated effector subset that co-expressed IFNγ, TNFα, and IL-10. By using IL-10 green fluorescent protein (gfp) transcriptional reporter mice, we identified that IL-10 was primarily expressed within CD4 T cells during acute infection in the lungs. IL10gfp expressing CD4 T cells were highly proliferative and characterized by the expression of multiple co-inhibitory receptors including PD-1 and LAG-3. When we analyzed acute γHV68 infection of IL-10 deficient mice, we found that IL-10 limits the frequency of both myeloid and effector CD4 T cell subsets in the infected lung, with minimal changes at a distant mucosal site. These data emphasize the unique insights that high-dimensional analysis can afford in investigating antiviral immunity, and provide new insights into the breadth, phenotype and function of IL-10 expressing effector CD4 T cells during acute virus infection.

56 **INTRODUCTION**

57 The gammaherpesviruses (γHVs) are a group of large dsDNA lymphotropic
58 viruses which include the human pathogens Epstein-Barr virus (EBV) and Kaposi's
59 sarcoma associated herpesvirus (KSHV), and the small animal model murine
60 gammaherpesvirus 68 (γHV68) (1-3). The γHVs establish a lifelong infection in their
61 host, with most infections in immunocompetent hosts asymptomatic. In contrast,
62 immunosuppressed individuals are at a significantly increased risk for the development
63 of a variety of chronic pathologies, including γHV-associated malignancies (4).

64 γHV infection is critically regulated by the immune system, and γHVs have
65 evolved numerous strategies to either subvert or avoid immune destruction, thereby
66 facilitating lifelong infection (5-7). Among these, IL-10 is a multifunctional cytokine that
67 downregulates the expression of multiple pro-inflammatory cytokines and cell surface
68 molecules, and can influence a wide array of immune cell types (8-10). IL-10 is a
69 frequent target of manipulation by the herpesviruses. Some γHVs, including Epstein-
70 Barr virus (EBV), encode their own IL-10 homolog (11, 12). In contrast, other viruses,
71 including murine gammaherpesvirus 68 (γHV68), inducing cellular IL-10 (13). IL-10 has
72 been reported to regulate multiple aspects of γHV68 infection. For instance, γHV68-
73 infected IL-10 deficient mice fail to control leukocytosis, have greater splenomegaly and
74 a reduced latent load (14), with these mice susceptible to an exacerbated inflammatory
75 bowel disease (15). IL-10 has been reported to be induced in B cells by the γHV68 M2
76 gene product (13). IL-10 expressing CD8 T cells have also been observed during
77 chronic γHV68 infection in mice depleted for CD4 T cells, an immunosuppressive
78 phenotype associated with chronic viral pathogenesis (16).

79 Based on the aforementioned studies, IL-10 regulates γHV68 infection. Here we
80 applied high-dimensional, single-cell analysis using mass cytometry (cytometry by time-
81 of-flight, CyTOF) (17) to define the breadth and cellular phenotype of IL-10 expressing
82 cells elicited during acute γHV68 infection. We further analyzed the genetic impact of IL-
83 10 in limiting γHV68 induced inflammation. These studies demonstrate the acute impact
84 of IL-10 on primary γHV infection in vivo and define effector CD4 T cells as a major cell
85 source of IL-10 during acute pulmonary infection.

86 **MATERIALS AND METHODS**

87

88 *Experimental samples.* Mice were obtained from the Jackson Laboratory and bred in-
89 house at the University of Colorado, including the C57BL/6J (B6, Jax stock #000664),
90 IL10-deficient (IL10KO, B6.129P2-*Il10*^{tm1Cgn}/J, Jax stock #002251), or IL10gfp
91 (B6.129S6-*Il10*^{tm1Flv}/J, Jax stock #008379) genotypes. Mice were intranasally infected
92 with $4x10^5$ plaque forming units (PFU) of wild-type (WT) murine gammaherpesvirus 68
93 (γHV68) in mice subjected to isoflurane induced anesthesia. Mice were used between 8-
94 15 weeks of age, with experimental cohorts age- and sex-matched. Mice were infected
95 with WT γHV68 (strain WUMS, ATCC VR-1465) (18), using either bacterial artificial
96 chromosome (BAC)-derived WT γHV68 (19) or WT γHV68.ORF73βla, which encodes a
97 fusion between ORF73 and the beta-lactamase gene (20). γHV68 was grown and
98 titered by plaque assay on NIH 3T12 fibroblasts as previously published (21). Mice
99 subjected to anti-CD3 antibody injection were injected intraperitoneally with 15 μg of
100 anti-CD3ε antibody (clone 145-2C11, BioXcell, Cat# BP0001-1) at 0 and 46 hours, with
101 spleens harvested at 50 hours post primary injection (22). Lung data in Figure 4 are
102 from a previously published dataset (23). All procedures were performed under
103 protocols approved by the Institutional Animal Care and Use Committee at the
104 University of Colorado Anschutz Medical Campus.

105

106 *Cell processing & antibody staining.* In-depth processing and staining protocol can be
107 found in (23). Briefly, lungs were perfused using 10-12 mL of phosphate buffered saline
108 (PBS), harvested, minced and enzymatically digested with collagenase D for 1 h at

109 37°C. Lungs and spleens were further subjected to mechanical disruption to generate
110 single-cell suspensions that were subjected to red blood cell lysis, and resuspended for
111 staining. Colons were surgically dissected, rinsed then vortexed in PBS to remove fecal
112 material, and incubated with PBS (Gibco) containing 15 mM HEPES (HyClone), 1 mM
113 EDTA (ThermoFisher) at room temperature for 15 minutes while samples were
114 vigorously vortexed, to remove intraepithelial lymphocytes. Colonic tissue was then
115 rinsed over a sieve, washed with ice cold PBS, minced and subjected to enzymatic
116 digestion using Collagenase VIII (100-200 units/mL final concentration, Sigma Aldrich)
117 diluted in RPMI 1640 (Gibco) supplemented with 5% fetal bovine serum, 15 mM
118 HEPES, and 1% penicillin/streptomycin. Enzymatic digestion was done for 20 minutes
119 at 37° C, under continuous vortexing. Enzymatic digestion was quenched using ice cold
120 RPMI 1640 with 5% fetal bovine serum. Colonic samples were washed with a 1:10,000
121 dilution of Benzonase® Nuclease (≥250 units/µL, Sigma Aldrich) in RPMI 1640 to
122 minimize cell aggregation, prior to staining with cisplatin as a live/dead discriminator.
123 For samples analyzed for intracellular cytokine staining, cells were pharmacologicaly
124 stimulated with PMA and ionomycin (ThermoFisher) in the presence of the Golgi
125 apparatus inhibitors brefeldin A and monensin (Biolegend) for 5 hours. Cells were
126 stained with cisplatin according to manufacturer's recommendations (Cell-ID™ Cisplatin,
127 Fluidigm), incubated with Fc receptor blocking Ab (clone 2.4G2, Tonbo Biosciences) for
128 10-20 min, stained with primary surface Abs for 30 min at 22°C or 15 min at 37°C and
129 15 min at 22°C. Secondary surface stains, to detect fluorophore conjugated antibodies,
130 were incubated for 20-30 min, and washed, with intracellular staining done using the
131 FoxP3 Fix/Perm Buffer kit (Thermo Fisher) for 2 hours or overnight at 4°C. Following

132 cell staining, cells were washed and resuspended in Intercalator (Cell-ID™ Intercalator-
133 Ir). A subset of experiments (Figures 1, 3, 4B, 4D, 4F, and 5) were subjected to isotopic
134 barcoding using the Fluidigm barcoding kit (Cell-ID™ 20-Plex Pd Barcoding Kit,
135 Fluidigm) prior to staining with the primary surface stains. Antibodies used for these
136 studies are listed in Tables 1-4B. All antibodies that were directly conjugated to
137 isotopically purified elements were obtained from Fluidigm. In each of the CyTOF
138 panels, a subset of antibodies were detected using a secondary detection approach,
139 with FITC, PE, APC or Biotin-conjugated antibodies (clone and source identified in
140 Tables 1-4B), detected using metal conjugated secondary antibodies against FITC, PE,
141 APC or Biotin (Fluidigm).
142
143 *CyTOF run and sample normalization/debarcoding*. Samples were collected on a Helios
144 mass cytometer (Fluidigm), with samples resuspended with equilibration beads to allow
145 for signal normalization, with the normalization software downloaded from the Nolan
146 laboratory GitHub page (https://github.com/nolanlab) (as in (23)). For experiments
147 where the samples were subjected to isotopic barcoding (Figures 1, 3, 4B, 4D, 4F, and
148 5) the debarcoding software was used following normalization
149 (https://github.com/nolanlab/single-cell-debarcoder). Normalized, debarcoded data were
150 subjected to traditional Boolean gating in FlowJo, identifying singlets (^{191}Iridium (Ir)+ ^{193}
151 Ir+) that were viable (^{195}Platinum(Pt)−). These events were then gated and exported for
152 downstream analysis. Additional Boolean gating was later performed for either CD45+
153 events or CD4+ T cell events, with gating criteria identified within each figure.
154

155 *PhenoGraph-based data analysis.* Manually gated singlet (^{191}Ir+ ^{193}Ir+) viable (^{195}Pt−)
156 events, or further gated populations, were imported into PhenoGraph, with relevant
157 clustering markers selected (28-35 cellular markers depending on the experiment; note
158 that markers used for gating imported populations were not used for clustering). All
159 parameters used for clustering are indicated in the associated Tables. PhenoGraph was
160 run with the following settings: i) files were merged using either the merge method
161 "min" (Figure 1, Figure 2A, and Figure 3), all (Figure 2B), or "ceiling" (Figure 3-5), ii) files
162 were transformed using the transformation method "cytofAsinh", iii) the "Rphenograph"
163 clustering method was chosen, coupled with the "tSNE" visualization method. All other
164 settings were automatically chosen, using default PhenoGraph settings.
165
166 *PhenoGraph-based visualization.* PhenoGraph-defined clusters were displayed on tSNE
167 plots within the R package "Shiny" (23). Within the "Shiny" application, cluster color was
168 altered or colored according to protein expression. Multiple .csv files were produced by
169 PhenoGraph, including "cluster median data" and "cluster cell percentage," which were
170 used to determine cluster phenotype, distribution between conditions, and statistical
171 significance between groups.
172
173 *Software used and statistical analysis.* Software for data analysis included: R studio
174 (Version 1.1.453), downloaded from the official R website (http://www.r-project.org/); the
175 Cytofkit package (Version 3.7), downloaded from Bioconductor
176 (https://Bioconductor.org/packages/release/bioc/html/cytofkit.html), Excel 16.15, FlowJo
177 10.4.2, GraphPad Prism 7.0c, and Adobe Illustrator CC 22.1. Cytofkit was opened using

178 R studio and XQuartz. Statistical significance was tested in GraphPad Prism using an
179 unpaired t test, with statistical significance as identified. For contexts in which we tested
180 statistical significance across all of the identified nodes/clusters (Fig. 4, 5), statistical
181 analysis was subjected to multiple comparison correction in GraphPad Prism.

182 **RESULTS**

183

184 ***High-dimensional analysis of effector CD4 T cells during primary γHV68 infection.***
185 γHV68 infection induces diverse effector CD4 T cell subsets throughout the course of
186 infection (24). To provide a high-dimensional analysis of effector CD4 T cell function
187 during primary infection, the lungs from γHV68 infected mice were harvested at 9 days
188 post-infection (dpi), subjected to pharmacological stimulation with PMA and ionomycin,
189 and analyzed by mass cytometry using a panel of 35 isotopically purified, metal
190 conjugated antibodies (Table 1). CD4 T cells were initially analyzed for expression of
191 IFNγ and TNFα expression, two hallmark effector cytokines elicited in antiviral CD4 T
192 cells. Between 40-60% of CD4 T cells harvested from infected lungs expressed either
193 IFNγ, TNFα, or co-expressed IFNγ and TNFα (Fig. 1A). IFNγ+TNFα+ effector CD4 T
194 cells were more frequent than either IFNγ+ or TNFα+ single positive cells (Fig. 1A). To
195 gain an unbiased perspective on the phenotypic diversity within these cytokine-defined
196 effector CD4 T cells, we next subjected these cell populations to the PhenoGraph
197 algorithm, to define cell clusters present in each cytokine-defined subset (25). By
198 clustering cells based on the expression of 30 proteins (including CD44, Tbet, IRF4 and
199 multiple co-inhibitory receptors, but not on CD3, CD4, MHCII, IFNγ or TNFα) (Table 1),
200 PhenoGraph defined 16 CD4 T cell clusters present in the virally infected lung (Fig. 1A-
201 B). The relative frequency of these cell clusters was notably affected by whether cells
202 expressed cytokines, and if so, which cytokines. Some clusters, depicted by shades of
203 gray in Fig. 1B, were present in relatively comparable frequencies across all subsets of
204 CD4 T cells, regardless of whether they expressed TNFα or IFNγ (e.g. cluster #10, a

205 population of CD4 T cells characterized by intermediate expression of GITR, PD-1 and
206 ICOS, Fig. 1C). In contrast, cluster #9 (depicted in black, Fig. 1B-C) contained CD44^{high}
207 IRF4^{mid} IL-2+ cells that were never found among the IFNγ-TNFα- subset of CD4 T cells.
208 Beyond these distinctions, there were two classes of cell clusters that were inversely
209 related: i) clusters enriched among IFNγ- CD4 T cells (depicted in pastel colors), and ii)
210 clusters enriched among IFNγ+ CD4 T cells (depicted in saturated colors, Fig. 1B-C).
211 Clusters enriched among IFNγ- cells were primarily CD44^{low} with limited expression of
212 notable phenotypic markers (Fig. 1C). Conversely, clusters enriched among IFNγ+
213 subsets (IFNγ+ or IFNγ+ TNFα+; clusters 8, 12 and 16) included: i) cluster #16, a
214 Tbet^{high} Lag3^{high} IRF4^{high} PD-1^{high} GITR+ CD25+ CTLA4+ ICOS+ population and ii)
215 cluster #8, a Tbet^{intermediate} IRF4^{high} IL-10^{high} GITR+ CTLA4+ PD-1+ ICOS+ population
216 (Fig. 1C). These data demonstrate that γHV68 elicits a diverse set of CD4 T cells during
217 primary infection, including the induction of an IFNγ+ IL-10+ effector CD4 T cell subset.
218
219 ***High-dimensional analysis of IL-10 expression as defined by an IL-10***
220 ***transcriptional reporter.*** Our initial analysis focused on the phenotypic diversity of
221 CD4 T cells elicited during virus infection, where we identified a prominent IL-10
222 producing effector CD4 T cell subset (cluster #8, Fig. 1C). To gain a broader
223 perspective on IL-10 expressing cells during primary virus infection, we next infected IL-
224 10 transcriptional reporter mice, in which the enhanced GFP gene is inserted 3' of the
225 endogenous Il10 gene (i.e. mice expressing the IL-10 *tiger* allele (26)). γHV68 infected
226 lungs were harvested at 6 dpi and subjected to mass cytometric analysis, where
227 samples were stained with a metal-conjugated, anti-GFP antibody to detect the IL-10

228 reporter (Table 2). As anticipated, γHV68 infection resulted in prominent changes in the
229 frequency and distribution of PhenoGraph-defined clusters relative to mock infected
230 lungs (Fig. 2A). When we analyzed the cellular distribution of the IL10gfp reporter,
231 IL10gfp expression was detected in a fraction of cells in infected lungs, primarily within
232 CD4 T cells (Fig. 2A).

233 Infection of IL-10 transcriptional reporter mice afforded a major advantage over
234 ICCS, as it measured IL-10 mRNA expression without the need for additional
235 pharmacologic stimuli which can alter cellular phenotype. We therefore focused on CD4
236 T cell phenotypes in either mock or virally-infected lungs using the PhenoGraph
237 clustering algorithm, which identified 16 CD4 T cell clusters across mock and γHV68
238 infected lungs. Virally-infected lungs had an increased number of CD4 T cells relative to
239 mock-infection, with a pronounced shift in CD4 T cell clusters (Fig. 2B) towards a
240 prominent $CD44^{high}$ $Ki67^{high}$ $ICOS^{high}$ $PD\text{-}1^{high}$ population (Fig. 2C). Within these virally-
241 elicited effector CD4 T cells, Lag3, Ly6C, and CD49b expression were expressed in
242 partially overlapping cell subsets (Fig. 2C). IL10gfp expression was detected in a subset
243 of virally-elicited effector CD4 T cells (Fig. 2C), specifically cluster #1 and #5 (Fig. 2D).
244 IL10gfp+ CD4 T cells between these two clusters shared a conserved $CD44^{high}$ $Ki67^{high}$
245 $ICOS^{+}$ $PD\text{-}1^{high}$ $Lag3^{high}$ $CD49b^{mid}$ phenotype, with $Ly6C^{high}$ and $Ly6C^{low}$ subsets. These
246 studies, using an IL-10 transcriptional reporter, demonstrate that CD4 T cells are a
247 primary source of IL-10 expression during acute γHV68 infection and further identify a
248 core phenotype associated with IL-10 expression within effector CD4 T cells.
249

250 ***γHV68 infection elicits a dominant IL10gfp expressing CD4 T cell population that***
251 ***differs from anti-CD3 antibody elicited IL10gfp expressing CD4 T cells.*** Multiple
252 CD4 T cell subsets can produce IL-10, including type 1 regulatory CD4 T cells, a
253 FoxP3- IL-10+ subset of CD4 T cells reported to co-express the cell surface proteins
254 Lag3 and CD49b (22). Based on the expression of Lag3 and CD49b in IL-10 expressing
255 CD4 T cells (Fig. 2C-D), we sought to compare these cells with Tr1 cells generated by
256 an established method. One published method to elicit Tr1 cells is the repeated injection
257 of anti-CD3 antibody into mice, a method associated with both polyclonal T cell
258 activation and the generation of Tr1 cells (22). In this context, Tr1 cells are found
259 especially in the small intestine, with a lower induction of these cells in other tissues
260 (26). To understand how virally induced IL-10+ CD4 T cells compare to IL-10+ CD4 T
261 cells elicited following anti-CD3 antibody injection, we compared CD4 T cells from the
262 lungs of γHV68 infected mice with CD4 T cells from the spleens of mice repeatedly
263 injected with anti-CD3 antibody. Cells were harvested and subjected to mass cytometric
264 analysis using a panel of 34 antibodies (Table 3). When CD4 T cells from these two
265 conditions were subjected to the PhenoGraph algorithm, we identified 20 clusters of
266 CD4 T cells (Fig. 3A). tSNE plots of CD4 T cells for each condition revealed largely non-
267 overlapping cell clusters, suggesting phenotypic divergence (Fig. 3A). Across both
268 conditions, five of twenty CD4 T cell clusters had above average expression of IL10gfp
269 (Fig. 3B). There were large differences in the frequency of IL10gfp+ cells among CD4 T
270 cells between conditions, with ~10% of CD4 T cells that were IL10gfp+ in the spleens of
271 anti-CD3 antibody injected mice, and ~50% of CD4 T cells that were IL10gfp+ in γHV68
272 infected lungs (Fig. 3C). When we analyzed the phenotype of IL10gfp+ clusters

273 between these two conditions, we found a significant phenotypic divergence. Within
274 anti-CD3 antibody injected mice, the highest frequency of IL10gfp+ cells were found
275 within a FoxP3+ regulatory T cell (Treg) cluster (Fig. 3D). In contrast, IL10gfp+ clusters
276 that were dominant in γHV68 infection were $CD44^{high}$ $Lag3^{high}$ $PD\text{-}1^{high}$ Tbet+ and
277 FoxP3-, suggesting they may be either Tr1 or Th1 cells (Fig. 3D). These data
278 emphasize the multiple potential cellular sources of IL-10 that can occur with diverse
279 stimuli and across tissues, and reveal that virus infection elicits a distinct effector T cell
280 phenotype when compared to anti-CD3 antibody injection.
281
282 ***IL-10 dependent regulation of γHV68 infection.*** To define how IL-10 regulates the
283 distribution and phenotype of immune cell subsets during γHV68 infection we used
284 mass cytometry to compare cellular composition and phenotype between γHV68
285 infected wild-type (B6) and IL-10 deficient (IL10KO) mice. This analysis focused on
286 cellular diversity among hematopoietic (CD45+) cells within the lungs and colon, with
287 tissues harvested from separate cohorts. Mass cytometry data were collected and
288 subjected to the PhenoGraph algorithm for clustering analysis. This analysis identified
289 29 cell clusters in lungs harvested from γHV68 infected mice, with 20 cell clusters
290 identified in the colons of γHV68 infected mice (Fig. 4A-B). Cell clusters were further
291 defined based on canonical lineage markers, to quantify the frequencies of distinct
292 leukocyte populations (Fig. 4C-D). When we compared cluster distribution between B6
293 and IL10KO mice, we found pronounced shifts in cellular distribution between B6 and
294 IL10KO infected lungs, particularly among CD4 T cells (Fig. 4C). In contrast, colons
295 from virally-infected mice had a very limited number of changes in cell clusters at this

296 time post-infection (Fig. 4D). Among the cell clusters present in infected lungs, IL10KO
297 mice had a significantly increased frequency in two cell clusters: i) PD-1+ Lag3+ CD4 T
298 cells (cluster #14), and ii) a small, but significant, increase in CD64+ cells (cluster #25)
299 (Fig. 4E). Colons from infected IL10KO mice had a selective increase in the frequency
300 of CD64+ cells characterized by a CD11b+ CD11c+ phenotype with variable CD103
301 expression (cluster #13) (Fig. 4F). Cluster #13 was unique among CD64+ clusters in
302 CD11c and CD103 expression relative to other CD64+ clusters in the colon (Fig. 4F).
303 These findings suggest that during acute γHV68 infection, IL-10 constrains the
304 expansion and/or survival of effector CD4 T cells in the lung, and further constrains the
305 frequency of CD64+ mononuclear phagocytic cells in both the lung and the colon.
306
307 ***IL-10 dependent regulation of effector CD4 T cell function during acute γHV68***
308 ***infection.*** Next, we sought to define how IL-10 regulates CD4 T cell effector function
309 during acute γHV68 infection, as revealed by intracellular cytokine staining analysis. We
310 compared CD4 T cell function between γHV68 infected B6 and IL10KO mice by ICCS
311 using mass cytometry. In contrast to the clustering analysis done in Fig. 1, CD4 T cells
312 for both genotypes were subjected to PhenoGraph-defined clustering using 32 markers
313 including IFNγ, TNFα and IL-10 (Table 1), identifying 16 unique clusters (Fig. 5A). CD4
314 T cells were predominantly $CD44^{high}$, consistent with a large effector CD4 T cell
315 population in virally-infected lungs at this time (Fig. 5B). 7 of the 16 PhenoGraph-
316 defined clusters showed expression of either IFNγ, TNFα and/or IL-10 (Fig. 5B), with
317 phenotypes ranging from single expression of IFNγ+ or TNFα+, coexpression of IFNγ+
318 and TNFα+, and triple expression of IFNγ+ TNFα+ and IL-10+ (Fig. 5B-C). When we

319 analyzed the frequency of CD4 T cells stratified by cytokine expression, we found that
320 B6 and IL10KO mice had comparable frequencies of TNFα+ single positive and IFNγ+
321 single positive CD4 T cells (Fig. 5C-D). As anticipated, IL10KO mice had no detectable
322 IL-10+ CD4 T cells (Fig. 5C-D). B6 mice had a significantly increased frequency of
323 cytokine negative CD4 T cells (IFNγ- TNFα- IL-10-) relative to IL10KO mice (Fig. 5C-D).
324 In contrast, IL10KO mice had a significantly increased frequency of IFNγ+ TNFα+
325 effector CD4 T cells (Fig. 5C-D). While IL10KO mice had an increased frequency of
326 IFNγ+ TNFα+ CD4 T cells relative to B6 mice, both genotypes had phenotypic diversity
327 within this cytokine producing subset, including cell subsets with partially overlapping
328 expression of CTLA-4, GITR, ICOS, Lag3 and PD-1 (Fig. 5E). These data demonstrate
329 that IL-10 constrains the magnitude of highly activated IFNγ+ TNFα+ effector CD4 T
330 cells during acute γHV68 infection, a population characterized by heterogeneous
331 expression of CTLA-4, GITR, ICOS, Lag3 and PD-1.

332 **DISCUSSION**

333 IL-10 is a multifunctional cytokine that critically shapes the magnitude and
334 activation status of the immune system in response to infection. In addition to its host
335 immunomodulatory functions, IL-10 is a frequent target of viral manipulation by the
336 herpesviruses (12, 13). Here we sought to investigate how γHV68, a small animal model
337 of gammaherpesvirus infection, intersects with IL-10, both in terms of what cells
338 produce IL-10 and how the overall immune response is influenced by IL-10 during acute
339 infection. For these studies, we have focused on acute, primary infection with γHV68,
340 seeking new insights through the use of high-dimensional mass cytometry (CyTOF)
341 analyses.

342 IL-10 is known to be produced by a large number of cell types, including CD4
343 and CD8 T cell subsets and B cells (8). Here we make use of IL-10eGFP transcriptional
344 reporter mice, and direct intracellular staining for IL-10 protein, to identify CD4 T cells as
345 a primary source of IL-10 production during acute γHV68 infection in the lung. IL-10+
346 CD4 T cells elicited during viral infection were associated with a highly activated effector
347 phenotype, characterized by high expression of CD44 with co-expression of the
348 cytokines IFNγ and TNFα. IL10gfp+ CD4 T cells were proliferating and characterized by
349 expression of PD-1, Lag3, ICOS, CD49b with variable expression of Ly6C. By querying
350 these cellular phenotypes using mass cytometry, we have further analyzed IL10gfp
351 expression across a wide range of leukocyte subsets. These studies demonstrated
352 focused expression of IL-10 within CD4 T cells in the infected lung with minimal IL-10
353 expression in other cell subsets at this time.

354 The expression of IL-10 within this highly activated effector CD4 T cells raises
355 the question of what effector subset(s) express IL-10 in this context. Our data
356 demonstrate that FoxP3+ Tregs are not a prominent source of IL-10 during acute γHV68
357 infection in the lung. Instead, IL-10+ CD4 T cells appear to be either: i) type 1
358 regulatory T cells, an IL-10 expressing, FoxP3 negative subset of CD4 T cells frequently
359 characterized by co-expression of CD49b and Lag3 (22), or ii) an IL-10 expressing Th1
360 subset (27-29). While the IL-10 expressing effector CD4 T cells that we identified here
361 co-express CD49b and Lag3, a proposed marker of Tr1 cells (22), recent studies have
362 emphasized that co-expression of CD49b and Lag3 is not a definitive marker of Tr1
363 cells (30, 31). Conversely, IFNγ+ Th1 cells have been reported to express IL-10 in a
364 variety of settings (32), and γHV68 induced IL-10+ effectors express Tbet, the canonical
365 Th1 transcription factor. Despite these observations, at this time there remains no
366 definitive marker that discriminates between Tr1 and Th1 cells. Alternatively, these
367 IFNγ+ IL-10+ expressing cells may represent a distinct effector CD4 T cell subset (33).
368 Recently, Eomesodermin was identified as a transcriptional regulator for IL-10+ effector
369 CD4 T cells, in both Tr1 cells (30) and a potentially distinct IFNγ+ IL-10+ effector CD4 T
370 cell (34). Whether IL-10+ CD4 T cells elicited during γHV68 infection express, and
371 require, Eomesodermin remains to be tested.
372 IL-10 regulates its effects through signals transduced by the heterodimeric IL-10
373 receptor, targeting multiple cell types (9). High-dimensional analysis of the immune
374 response after γHV68 infection identified a wide spectrum of cells in infected lung and
375 colon, a phenotypic diversity readily characterized through use of the PhenoGraph
376 clustering algorithm and visualized by the tSNE data dimensionality method. When we

377 compared cellular and phenotypic diversity between B6 and IL10KO mice, we found a
378 pronounced increase in the frequency of a PD-1+ Lag3+ CD4 T cell subset and an
379 exaggerated induction of IFNγ+ TNFα+ effector CD4 T cells. We further found evidence
380 for changes in CD64+ populations in both the infected lung and colon. While IL-10 may
381 directly regulate effector CD4 T cell function (35, 36), CD4 T cell differentiation and
382 effector function may also occur due to altered myeloid function(s) (8, 10, 37, 38).
383 Future studies using targeted disruption of IL-10 signaling in myeloid cells (e.g.
384 macrophages, dendritic cells) and T cells will be required to determine whether IL-10
385 directly or indirectly modulates effector CD4 T cell differentiation during γHV68 infection.
386 Regardless of the molecular basis of this phenoype, the increased frequency of PD-1+
387 Lag3+ effector CD4 T cells in IL-10 deficient mice suggests that co-inhibitory receptor
388 expression may function as a compensatory mechanism to constrain pathogenic CD4 T
389 cell function in the absence of IL-10.
390 Beyond insights on IL-10 dependent regulation during γHV68 infection, these
391 studies demonstrate the power of high-dimensional approaches, such as mass
392 cytometry, to investigate the regulation of the immune response at a global level. By
393 applying mass cytometry to CD4 T cells, our studies provide direct evidence for
394 extensive phenotypic diversity of antiviral effector CD4 T cells elicited during primary
395 viral infection. We anticipate that combining mass cytometry-based studies with host
396 and viral genetics will afford new insights into the underpinnings of antiviral CD4 T cell
397 function.
398

399 **FIGURE LEGENDS**

400

401 **Figure 1. High-dimensional analysis of CD4 T cells elicited during primary γHV68**
402 **infection.** Mass cytometric analysis of cells recovered from the lungs of γHV68 infected
403 C57BL/6J (B6) mice at 9 dpi, subjected to intracellular cytokine staining (ICCS)
404 analysis, using a 35 antibody panel (Table 1). Data were gated on viable CD4 T cells,
405 defined as ^{191}Ir+ ^{193}Ir+ ^{195}Pt- ^{152}CD3ε+ ^{172}CD4+ ^{174}MHC II- events, where numbers
406 indicate isotopic mass for each measured parameter. (A) Analysis of IFNγ and TNFα
407 production from CD4 T cells subjected to pharmacologic stimulation with PMA and
408 ionomycin. The mean ± SEM for each population is identified in each quadrant. Events
409 in each quadrant were further analyzed using the PhenoGraph algorithm and plotted
410 using the tSNE dimensionality reduction algorithm. Events were imported into
411 PhenoGraph and clustered on 8,320 events total and 30 markers (clustering parameters
412 identified in Table 1). In total, 16 clusters were identified, with clusters colored by cluster
413 ID and displayed on tSNE plots. (B) Distribution of PhenoGraph-defined clusters within
414 CD4 T cells, stratified by expression of IFNγ and TNFα. Each pie chart is subdivided
415 into clusters that are equally represented in IFNγ- and IFNγ+ CD4 T cells (shades of
416 gray), clusters that are enriched in IFNγ- CD4 T cells (pastel colors), clusters that are
417 enriched only in cytokine producing CD4 T cells (black), and clusters that are enriched
418 in IFNγ+ CD4 T cells (saturated colors) as defined in the key. Right panel shows events
419 depicted using tSNE, where each cluster is colored according to the cytokine profile
420 subsets (see key). (C) Phenotypic marker expression (in columns) of PhenoGraph-
421 defined clusters (in rows), stratified by their enrichment as a function of cytokine profile.

422 Clusters are stratified as in panel B. Data are from virally infected B6 lungs (n=4 mice)
423 harvested 9 dpi, with cells stimulated with PMA and ionomycin for five hours prior to
424 antibody staining.
425
426 **Figure 2. High-dimensional analysis of IL10gfp expression during acute γHV68**
427 **infection in the lung.** Mass cytometric analysis of cells recovered from the lungs of
428 γHV68 infected IL10gfp mice at 6 dpi. Files were normalized, with events gated on (A)
429 total viable, single cells (defined as ^{191}Ir+ ^{193}Ir+ ^{195}Pt-) or (B-D) viable, CD4+ T cells
430 (defined as ^{191}Ir+ ^{193}Ir+ ^{195}Pt- ^{152}CD3ε+ ^{172}CD4+ ^{174}MHC II-) prior to analysis, where
431 numbers indicate isotopic mass for each measured parameter. (A) PhenoGraph
432 analysis of cellular phenotypes in mock and virally-infected lung (28,924 events total),
433 clustered based on 29 markers (Table 2), identified 34 unique clusters, with cluster
434 phenotype defined according to the indicated lineage markers. The “CD45+” cluster was
435 defined by its expression of CD45+ and absence of other lineage defining markers. The
436 right panel of A shows all viable, singlet events from mock- and virally-infected lungs,
437 with events colored according to IL10gfp expression. The green boundary line defines
438 CD4+ T cells. (B) Mass cytometric analysis and PhenoGraph-based cell clustering of
439 CD4+ T cells (5,464 events total, clustered based on 26 markers, excluding CD3, CD4,
440 and MHC II, Table 2). In total 16 unique clusters were identified, visualized on a tSNE
441 plot (left). The number and frequency of CD4 T cell clusters is shown in the right panel,
442 with pie charts sized proportionally to the relative cell number of CD4 T cells in mock or
443 virus infected lung. (C) Phenotypic analysis of CD4 T cells, with events predominantly in
444 mock infection denoted with a gray boundary and events predominantly in virus

445 infection denoted with a red boundary. Data depict CD4 T cells plotted according to
446 tSNE1 and tSNE2, as in panel B, with individual plots depicting relative protein
447 expression for the identified marker portrayed by color intensity, with range of
448 expression indicated on the bottom of each panel. Panels are ordered based on the
449 frequency of positive events. (D) Summary of CD4 T cell clusters (in columns) that differ
450 between mock and γHV68 infected lungs, with protein expression denoted in rows (gray
451 shading scaled relative to expression level). Data are from the lungs of a mock- or
452 γHV68-infected mouse harvested at 6 dpi, with panel D quantifying the frequency of
453 events in each cluster as a percentage of CD4+ T cells.
454
455 **Figure 3. γHV68 infection elicits a dominant IL10gfp expressing CD4 T cell**
456 **population that differs relative to IL10gfp expressing CD4 T cells in anti-CD3**
457 **antibody injected mice.** Mass cytometric analysis of cells recovered from IL10gfp
458 mice, comparing CD4 T cell phenotypes between the spleens of anti-CD3 antibody
459 injected mice with the lungs of γHV68 infected mice harvested at 6 dpi. Files were
460 normalized and gated on viable, CD4+ T cells (defined as ^{191}Ir+ ^{193}Ir+ ^{195}Pt- ^{152}CD3ε+
461 ^{172}CD4+ ^{209}MHC II-) prior to analysis, where numbers indicate isotopic mass for each
462 measured parameter. (A) PhenoGraph analysis of CD4 T cells, comparing anti-CD3
463 antibody injected versus γHV68 infected samples (75,483 events total, clustered on 33
464 markers, excluding CD3, CD4, and MHC II, Table 3), identified 20 unique clusters, each
465 denoted with a distinct color. (B) PhenoGraph-defined CD4 T cell clusters were ranked
466 based on IL10gfp expression, with 5 clusters having higher than average IL10gfp
467 expression identified in red text. Figure insets depict all events from panel A, colored

468 according to (left panel) IL10gfp expression, or (right panel) cluster ID for 5 IL10gfp+
469 clusters. (C) The frequencies of CD4 T cell clusters are shown for both conditions, with
470 focused analysis on the distribution of IL10gfp+ clusters identified by shaded gray
471 extensions and pie charts on either side. Pie charts denote the frequencies of IL10gfp+
472 events in each condition, with pie charts sized according to the relative number of
473 IL10gfp+ events present in each condition. (D) Comparison of median protein
474 expression within IL10gfp+ CD4 T cell clusters in either anti-CD3 antibody injected
475 spleens and/or γHV68 infected lungs. Cellular markers are ordered by range in median
476 expression between clusters, from greatest to least in value. Data are from IL10gfp
477 mice, using either spleens from mice that were injected with an anti-CD3 antibody
478 (injected with antibody at 0 and 46 hours, with harvest at 50 hours, n=4 mice) or lungs
479 from γHV68 infected (n=5 mice) harvested at 6 dpi.
480
481 **Figure 4. High dimensional analysis of IL-10 dependent regulation of the antiviral**
482 **response in the lung and the colon.** Mass cytometric analysis of cells recovered from
483 lungs (A,C,E) or colons (B,D,F) of γHV68 infected B6 or IL10KO mice harvested at 9
484 dpi. Files were normalized and gated on viable, single CD45+ cells (defined as ^{191}Ir+
485 ^{193}Ir+ ^{195}Pt- ^{89}CD45+) prior to analysis, where numbers indicate isotopic mass for each
486 measured parameter. (A, B) PhenoGraph analysis of CD45+ cells from (A) lungs or (B)
487 colons of γHV68 infected B6 or IL10KO mice. Clustering was done on 4,344 events per
488 file (34,752 total), with clustering in the lung based on 34 markers (29 clusters identified,
489 Table 4A) and clustering in the colon based on 36 markers (20 clusters identified, Table
490 4B); lungs and colons were harvested from separate cohorts. PhenoGraph-defined

491 clusters are colored according to cluster ID. (C,D) Definition of cellular phenotypes
492 across PhenoGraph-defined clusters, according to the indicated lineage markers, with
493 distinct cell types given unique colors. “CD45+ MHC II+” and “CD45+ MHC II-” clusters
494 were defined by exclusion from other phenotypes. (E,F) Identification of clusters with
495 statistically significant differences in frequency between B6 and IL10KO infected (E)
496 lungs and (F) colons, showing cluster frequencies (left panel) and expression for the
497 identified parameters within the identified cluster (right panel). In the right panel of E,
498 plotted events are CD4+ T cells identified in panel C. In the right panel of F, plotted
499 events are the dominant CD64+ cell clusters identified in panel D. Parameters with a
500 different maximum scale value between B6 and IL10KO are identified by italicized text
501 and an asterisk. Data are from γHV68 infected B6 and IL10KO lungs (n=4 mice per
502 genotype) and colons (n=4 mice per genotype) harvested 9 dpi. Data depict mean ±
503 SEM with individual symbols indicating values from independent samples. All samples
504 were analyzed for statistical significance using unpaired t tests, corrected for multiple
505 comparisons using the Holm-Sidak method, with statistical significance denoted as *
506 $p<0.05$, ** $p<0.01$, ***$p<0.001$.
507
508 **Figure 5. High-dimensional analysis of effector CD4 T cell function following**
509 **γHV68 infection in B6 and IL10KO mice.** Mass cytometric analysis of cells recovered
510 from lungs of γHV68 infected B6 or IL10KO mice harvested at 9 dpi, with cells subjected
511 to pharmacologic stimulation for intracellular cytokine staining analysis (ICCS), using a
512 35 antibody panel (Table 1). Files were normalized, with data gated on viable CD4 T
513 cells, defined as ^{191}Ir+ ^{193}Ir+ ^{195}Pt- ^{152}CD3ε+ ^{172}CD4+ ^{174}MHC II- events, where numbers

514 indicate isotopic mass for each measured parameter. (A) CD4 T cells were imported
515 into PhenoGraph and clustered on 33,022 total events (3,669 events from each file) and
516 32 markers (excluding CD3, CD4, and MHC II, Table 1), identifying 16 unique clusters
517 portrayed on a tSNE plot. (B) All events from panel A are colored by CD44, IFNγ, TNFα,
518 and IL-10 expression. (C) Events from panel A colored based on their cytokine profile,
519 stratified based on IFNγ, TNFα, and IL-10 expression. (D) Frequency of CD4 T cells in
520 virally-infected B6 and IL10KO mice. (E) Comparison of CTLA-4, GITR, ICOS, Lag3,
521 and PD-1 expression across CD4 T cells from B6 (top row) or IL10KO (bottom row)
522 mice, where IFNγ+ TNFα+ CD4 T cells were identified by a green boundary line.
523 Parameters with a different maximum scale value between B6 and IL10KO are
524 identified by italicized text and an asterisk. Data from virally infected lungs of B6 (n=4)
525 and IL10KO (n= 5) mice harvested 9 dpi, with cells stimulated with PMA and ionomycin
526 for five hours prior to ICCS. Data for B6 mice were also included in Figure 1, subjected
527 to different clustering parameters (as outlined in Table 1). Data show mean ± SEM with
528 individual symbols denoting individual mice, with statistical analysis done by unpaired t
529 test, corrected for multiple comparisons using the Holm-Sidak method. Statistical
530 significance denoted by **, $p<0.01$ and ***, $p<0.001$. ns, not significant.

ACKNOWLEDGEMENTS

The authors acknowledge Melissa Ledezma for technical assistance, Kristina Terrell, Christine Childs, and Karen Helm for technical support for CyTOF studies including machine operation and management of the CU CyTOF antibody bank, and the CyTOF User Group at the University of Colorado Anschutz Medical Campus for their ongoing collaboration and insights.

DISCLOSURES

The authors have no financial conflicts of interest.

AUTHOR CONTRIBUTIONS

E.T.C. and L.F.v.D. conceived and obtained funding for the studies. L.M.O. and R.E.K. performed all experiments, with input on CyTOF experimental design from A.K.K. and E.T.C. A.K.K. performed all data analysis, data visualization, and wrote the initial manuscript draft with input from E.T.C. A.K.K., L.F.v.D. and E.T.C. wrote the manuscript with input from all authors.

547 **REFERENCES**

548

549 1. Longnecker, R. M., Kieff, E., Cohen, J.I. 2013. Epstein-Barr Virus. In *Fields*
550 *Virology*, 6th ed.

551 2. Dittmer, D. P., and B. Damania. 2016. Kaposi sarcoma-associated herpesvirus:
552 immunobiology, oncogenesis, and therapy. *J Clin Invest* 126: 3165-3175.

553 3. Barton, E., P. Mandal, and S. H. Speck. 2011. Pathogenesis and host control of
554 gammaherpesviruses: lessons from the mouse. *Annu Rev Immunol* 29: 351-397.

555 4. Cesarman, E. 2014. Gammaherpesviruses and lymphoproliferative disorders.
556 *Annu Rev Pathol* 9: 349-372.

557 5. Mariggio, G., S. Koch, and T. F. Schulz. 2017. Kaposi sarcoma herpesvirus
558 pathogenesis. *Philos Trans R Soc Lond B Biol Sci* 372.

559 6. Ressing, M. E., M. van Gent, A. M. Gram, M. J. Hooykaas, S. J. Piersma, and E.
560 J. Wiertz. 2015. Immune Evasion by Epstein-Barr Virus. *Curr Top Microbiol*
561 *Immunol* 391: 355-381.

562 7. Hu, Z., and E. J. Usherwood. 2014. Immune escape of gamma-herpesviruses
563 from adaptive immunity. *Rev Med Virol* 24: 365-378.

564 8. Saraiva, M., and A. O'Garra. 2010. The regulation of IL-10 production by immune
565 cells. *Nat Rev Immunol* 10: 170-181.

566 9. Ouyang, W., S. Rutz, N. K. Crellin, P. A. Valdez, and S. G. Hymowitz. 2011.
567 Regulation and functions of the IL-10 family of cytokines in inflammation and
568 disease. *Annu Rev Immunol* 29: 71-109.

569 10. Rojas, J. M., M. Avia, V. Martin, and N. Sevilla. 2017. IL-10: A Multifunctional
570 Cytokine in Viral Infections. *J Immunol Res* 2017: 6104054.

571 11. Hsu, D. H., R. de Waal Malefyt, D. F. Fiorentino, M. N. Dang, P. Vieira, J. de
572 Vries, H. Spits, T. R. Mosmann, and K. W. Moore. 1990. Expression of
573 interleukin-10 activity by Epstein-Barr virus protein BCRF1. *Science* 250: 830-
574 832.
575 12. Moore, K. W., P. Vieira, D. F. Fiorentino, M. L. Trounstine, T. A. Khan, and T. R.
576 Mosmann. 1990. Homology of cytokine synthesis inhibitory factor (IL-10) to the
577 Epstein-Barr virus gene BCRFI. *Science* 248: 1230-1234.
578 13. Siegel, A. M., J. H. Herskowitz, and S. H. Speck. 2008. The MHV68 M2 protein
579 drives IL-10 dependent B cell proliferation and differentiation. *PLoS Pathog* 4:
580 e1000039.
581 14. Peacock, J. W., and K. L. Bost. 2001. Murine gammaherpesvirus-68-induced
582 interleukin-10 increases viral burden, but limits virus-induced splenomegaly and
583 leukocytosis. *Immunology* 104: 109-117.
584 15. Nelson, D. A., C. C. Petty, and K. L. Bost. 2009. Infection with murine
585 gammaherpesvirus 68 exacerbates inflammatory bowel disease in IL-10-deficient
586 mice. *Inflamm Res* 58: 881-889.
587 16. Molloy, M. J., W. Zhang, and E. J. Usherwood. 2011. Suppressive CD8+ T cells
588 arise in the absence of CD4 help and compromise control of persistent virus. *J*
589 *Immunol* 186: 6218-6226.
590 17. Spitzer, M. H., and G. P. Nolan. 2016. Mass Cytometry: Single Cells, Many
591 Features. *Cell* 165: 780-791.

592 18. Virgin, H. W. t., P. Latreille, P. Wamsley, K. Hallsworth, K. E. Weck, A. J. Dal
593 Canto, and S. H. Speck. 1997. Complete sequence and genomic analysis of
594 murine gammaherpesvirus 68. *J Virol* 71: 5894-5904.
595 19. Adler, H., M. Messerle, M. Wagner, and U. H. Koszinowski. 2000. Cloning and
596 mutagenesis of the murine gammaherpesvirus 68 genome as an infectious
597 bacterial artificial chromosome. *J Virol* 74: 6964-6974.
598 20. Nealy, M. S., C. B. Coleman, H. Li, and S. A. Tibbetts. 2010. Use of a virus-
599 encoded enzymatic marker reveals that a stable fraction of memory B cells
600 expresses latency-associated nuclear antigen throughout chronic
601 gammaherpesvirus infection. *J Virol* 84: 7523-7534.
602 21. Diebel, K. W., L. M. Oko, E. M. Medina, B. F. Niemeyer, C. J. Warren, D. J.
603 Claypool, S. A. Tibbetts, C. D. Cool, E. T. Clambey, and L. F. van Dyk. 2015.
604 Gammaherpesvirus small noncoding RNAs are bifunctional elements that
605 regulate infection and contribute to virulence in vivo. *MBio* 6: e01670-01614.
606 22. Gagliani, N., C. F. Magnani, S. Huber, M. E. Gianolini, M. Pala, P. Licona-Limon,
607 B. Guo, D. R. Herbert, A. Bulfone, F. Trentini, C. Di Serio, R. Bacchetta, M.
608 Andreani, L. Brockmann, S. Gregori, R. A. Flavell, and M. G. Roncarolo. 2013.
609 Coexpression of CD49b and LAG-3 identifies human and mouse T regulatory
610 type 1 cells. *Nat Med* 19: 739-746.
611 23. Kimball, A. K., L. M. Oko, B. L. Bullock, R. A. Nemenoff, L. F. van Dyk, and E. T.
612 Clambey. 2018. A Beginner's Guide to Analyzing and Visualizing Mass
613 Cytometry Data. *J Immunol* 200: 3-22.

614 24. Hu, Z., M. A. Blackman, K. M. Kaye, and E. J. Usherwood. 2015. Functional
615 heterogeneity in the CD4+ T cell response to murine gamma-herpesvirus 68. *J*
616 *Immunol* 194: 2746-2756.
617 25. Levine, J. H., E. F. Simonds, S. C. Bendall, K. L. Davis, A. D. Amir el, M. D.
618 Tadmor, O. Litvin, H. G. Fienberg, A. Jager, E. R. Zunder, R. Finck, A. L.
619 Gedman, I. Radtke, J. R. Downing, D. Pe'er, and G. P. Nolan. 2015. Data-Driven
620 Phenotypic Dissection of AML Reveals Progenitor-like Cells that Correlate with
621 Prognosis. *Cell* 162: 184-197.
622 26. Kamanaka, M., S. T. Kim, Y. Y. Wan, F. S. Sutterwala, M. Lara-Tejero, J. E.
623 Galan, E. Harhaj, and R. A. Flavell. 2006. Expression of interleukin-10 in
624 intestinal lymphocytes detected by an interleukin-10 reporter knockin tiger
625 mouse. *Immunity* 25: 941-952.
626 27. Sun, J., R. Madan, C. L. Karp, and T. J. Braciale. 2009. Effector T cells control
627 lung inflammation during acute influenza virus infection by producing IL-10. *Nat*
628 *Med* 15: 277-284.
629 28. Weiss, K. A., A. F. Christiaansen, R. B. Fulton, D. K. Meyerholz, and S. M.
630 Varga. 2011. Multiple CD4+ T cell subsets produce immunomodulatory IL-10
631 during respiratory syncytial virus infection. *J Immunol* 187: 3145-3154.
632 29. Parish, I. A., H. D. Marshall, M. M. Staron, P. A. Lang, A. Brustle, J. H. Chen, W.
633 Cui, Y. C. Tsui, C. Perry, B. J. Laidlaw, P. S. Ohashi, C. T. Weaver, and S. M.
634 Kaech. 2014. Chronic viral infection promotes sustained Th1-derived
635 immunoregulatory IL-10 via BLIMP-1. *J Clin Invest* 124: 3455-3468.

636 30. Zhang, P., J. S. Lee, K. H. Gartlan, I. S. Schuster, I. Comerford, A. Varelias, M.
637 A. Ullah, S. Vuckovic, M. Koyama, R. D. Kuns, K. R. Locke, K. J. Beckett, S. D.
638 Olver, L. D. Samson, M. Montes de Oca, F. de Labastida Rivera, A. D. Clouston,
639 G. T. Belz, B. R. Blazar, K. P. MacDonald, S. R. McColl, R. Thomas, C. R.
640 Engwerda, M. A. Degli-Esposti, A. Kallies, S. K. Tey, and G. R. Hill. 2017.
641 Eomesodermin promotes the development of type 1 regulatory T (TR1) cells. *Sci*
642 *Immunol* 2.
643 31. Huang, W., S. Solouki, C. Carter, S. G. Zheng, and A. August. 2018. Beyond
644 Type 1 Regulatory T Cells: Co-expression of LAG3 and CD49b in IL-10-
645 Producing T Cell Lineages. *Front Immunol* 9: 2625.
646 32. Jankovic, D., D. G. Kugler, and A. Sher. 2010. IL-10 production by CD4+ effector
647 T cells: a mechanism for self-regulation. *Mucosal Immunol* 3: 239-246.
648 33. Haringer, B., L. Lozza, B. Steckel, and J. Geginat. 2009. Identification and
649 characterization of IL-10/IFN-gamma-producing effector-like T cells with
650 regulatory function in human blood. *J Exp Med* 206: 1009-1017.
651 34. Gruarin, P., S. Maglie, M. De Simone, B. Haringer, C. Vasco, V. Ranzani, R.
652 Bosotti, J. S. Noddings, P. Larghi, F. Facciotti, M. L. Sarnicola, M. Martinovic, M.
653 Crosti, M. Moro, R. L. Rossi, M. E. Bernardo, F. Caprioli, F. Locatelli, G. Rossetti,
654 S. Abrignani, M. Pagani, and J. Geginat. 2018. Eomesodermin controls a unique
655 differentiation program in human IL-10 and IFN-gamma coproducing regulatory T
656 cells. *Eur J Immunol*.
657 35. Sun, J., A. Cardani, A. K. Sharma, V. E. Laubach, R. S. Jack, W. Muller, and T.
658 J. Braciale. 2011. Autocrine regulation of pulmonary inflammation by effector T-

659 cell derived IL-10 during infection with respiratory syncytial virus. *PLoS Pathog* 7:
660 e1002173.
661 36. Brockmann, L., N. Gagliani, B. Steglich, A. D. Giannou, J. Kempski, P. Pelczar,
662 M. Geffken, B. Mfarrej, F. Huber, J. Herkel, Y. Y. Wan, E. Esplugues, M.
663 Battaglia, C. F. Krebs, R. A. Flavell, and S. Huber. 2017. IL-10 Receptor
664 Signaling Is Essential for TR1 Cell Function In Vivo. *J Immunol* 198: 1130-1141.
665 37. Mittal, S. K., and P. A. Roche. 2015. Suppression of antigen presentation by IL-
666 10. *Curr Opin Immunol* 34: 22-27.
667 38. Ip, W. K. E., N. Hoshi, D. S. Shouval, S. Snapper, and R. Medzhitov. 2017. Anti-
668 inflammatory effect of IL-10 mediated by metabolic reprogramming of
669 macrophages. *Science* 356: 513-519.
670

CD4 T cells (191+ 193+ 195- CD3+ CD4+ MHCII- events), stimulated for ICCS

A.

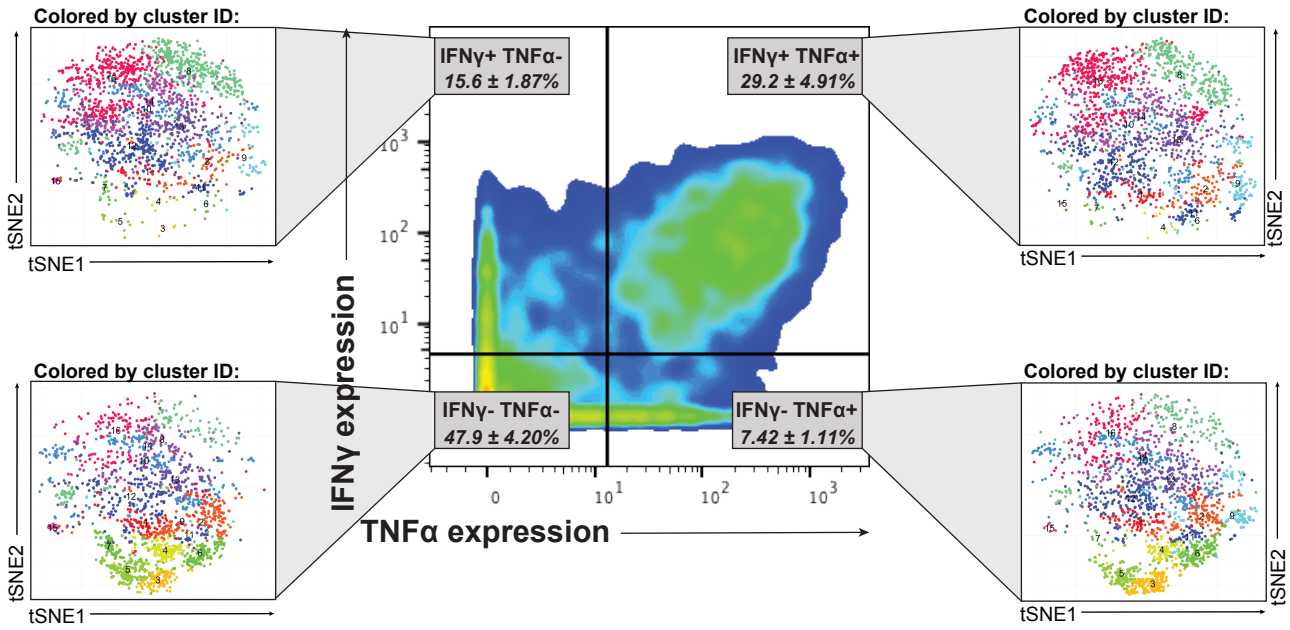

B.

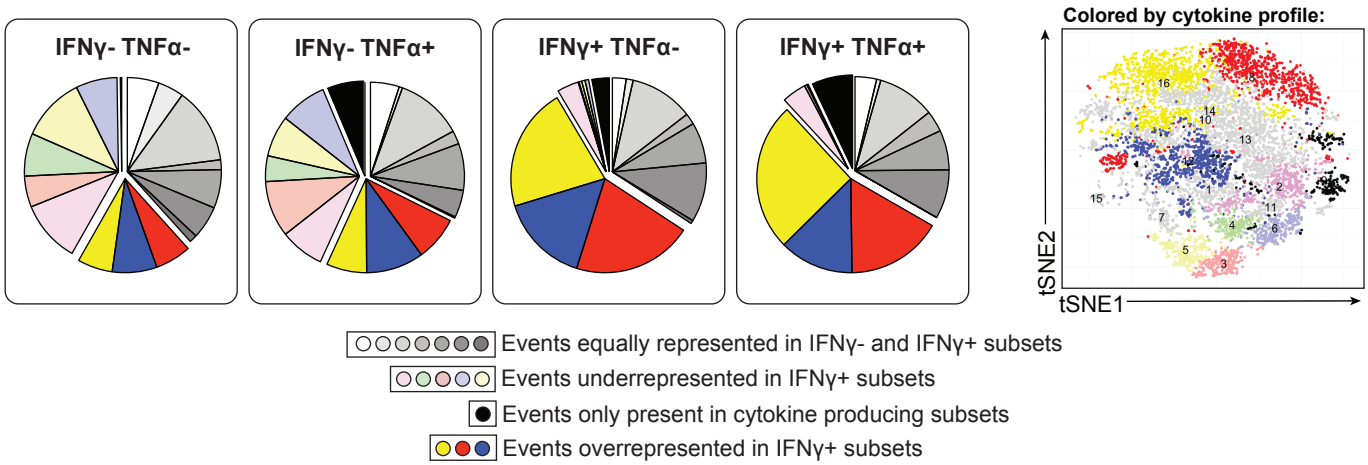

C.

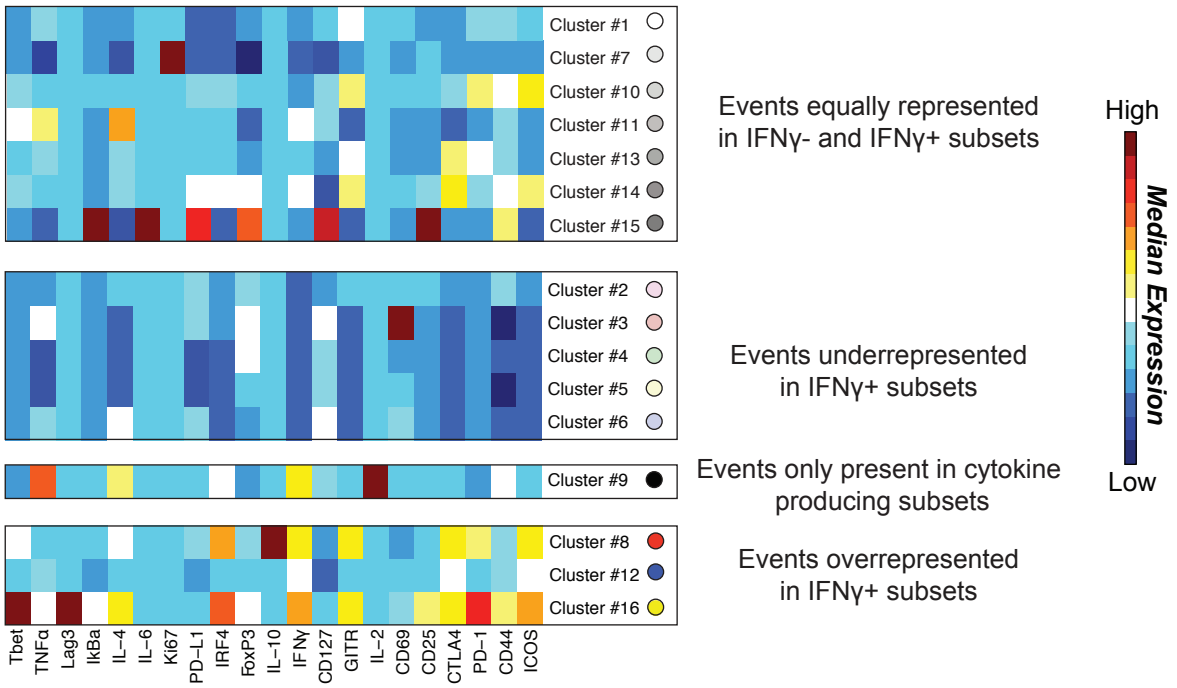

Kimball et al
Figure 1

Live, Singlet Events (191+ 193+ 195- events)

A.

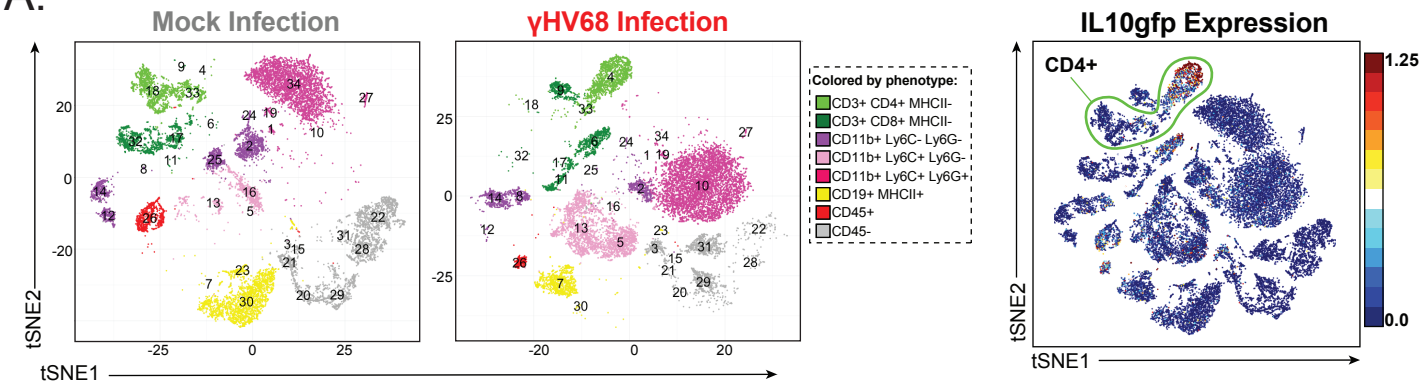

CD4 T cells (191+ 193+ 195- CD3+ CD4+ MHCII- events)

B.

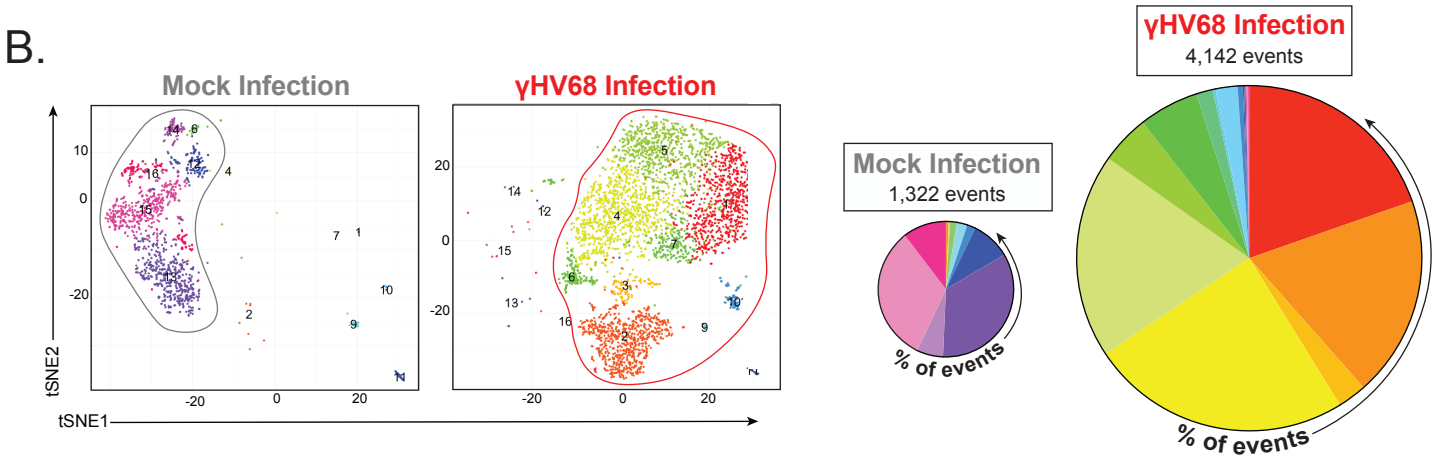

C.

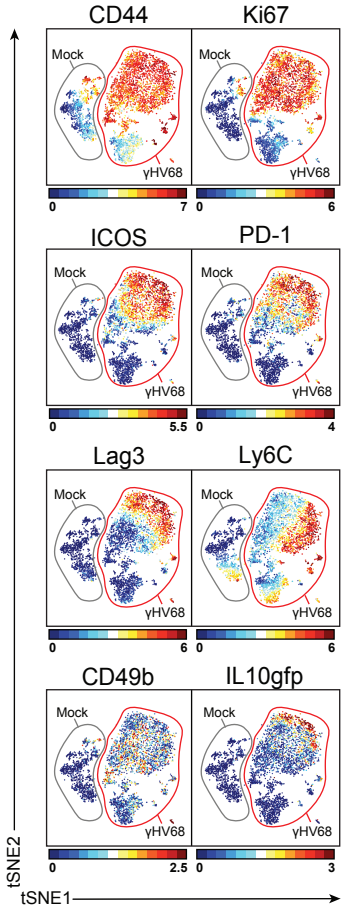

D.

	Enriched in mock infection				Enriched in γHV68 infection				
Cluster ID	#12	#13	#14	#15	#1	#2	#4	#5	
Protein Markers	Hi	Lo	Hi	Lo	Hi	Mid	Hi	Hi	CD44
	Hi	Lo	Lo	Lo	Hi	Lo	Hi	Hi	Ki67
	Lo	Lo	Lo	Lo	Mid	Lo	Mid	Hi	ICOS
	Lo	Lo	Lo	Lo	Hi	Lo	Mid	Hi	PD-1
	Lo	Lo	Lo	Lo	Hi	Lo	Lo	Hi	Lag3
	Lo	Mid	Lo	Lo	Hi	Mid	Mid	Lo	Ly6C
	Lo	Lo	Mid	Lo	Mid	Lo	Mid	Mid	CD49b
	-	-	-	-	+/-	-	-	+/-	IL10gfp
	9.4%	34.2%	6.3%	32.7%	0.1%	0.6%	0.3%	0.0%	% of mock
	0.1%	0.1%	0.1%	0.1%	19.7%	18.8%	24.5%	19.2%	% of infected

Kimball et al
Figure 2

CD4 T cells (191+ 193+ 195- CD3+ CD4+ MHCII- events)

A.

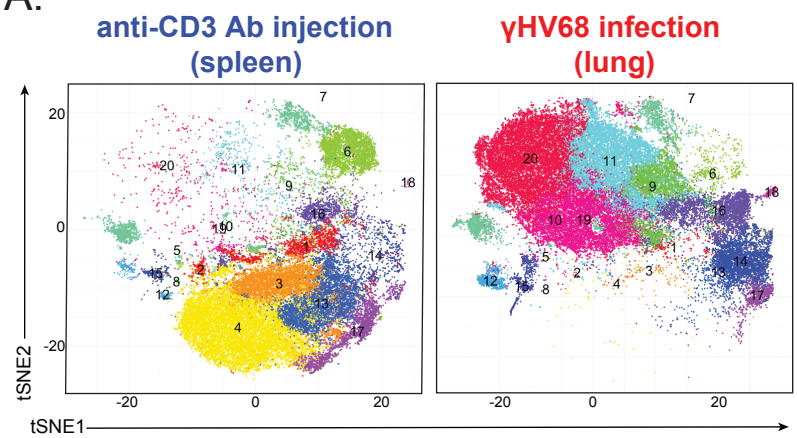

B.

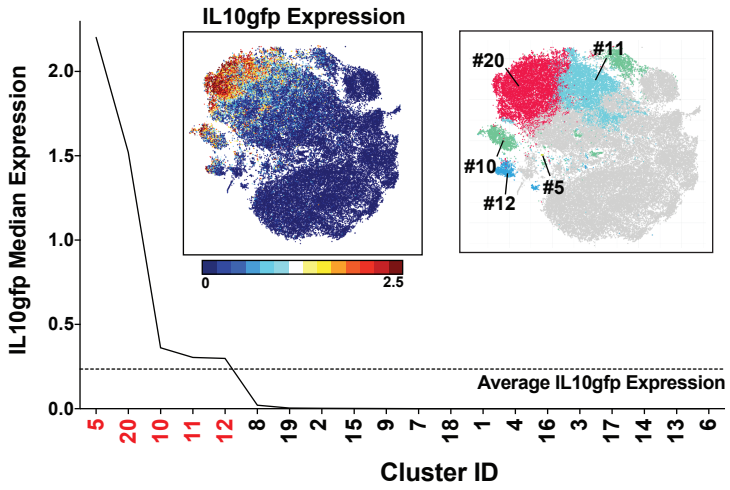

C.

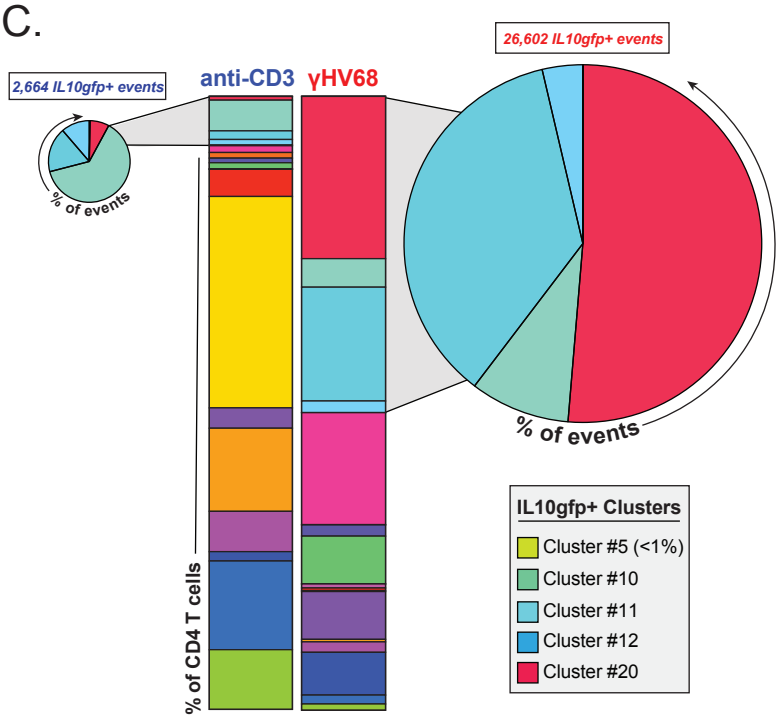

D.

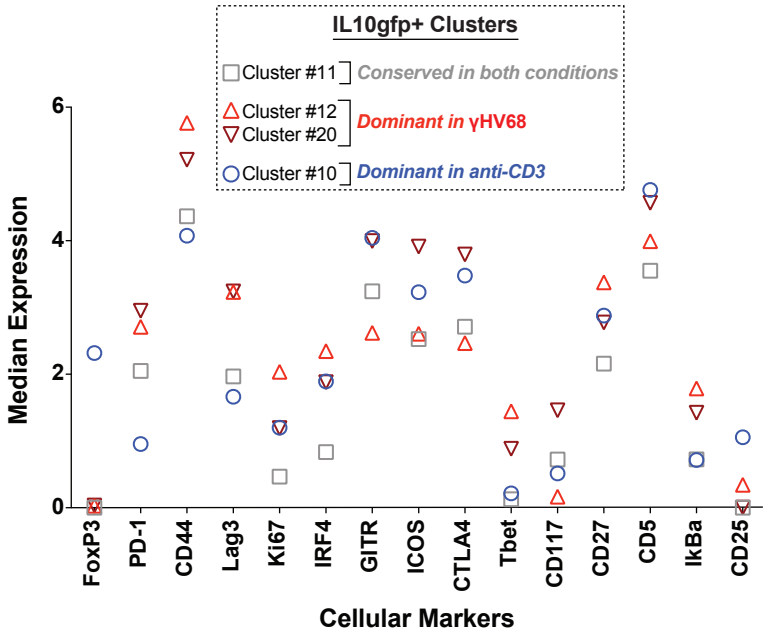

Kimball et al
Figure 3

***Lung:* Live, Singlet, CD45+ Events**
(191+ 193+ 195- CD45+ events)

***Colon:* Live, Singlet, CD45+ Events**
(191+ 193+ 195- CD45+ events)

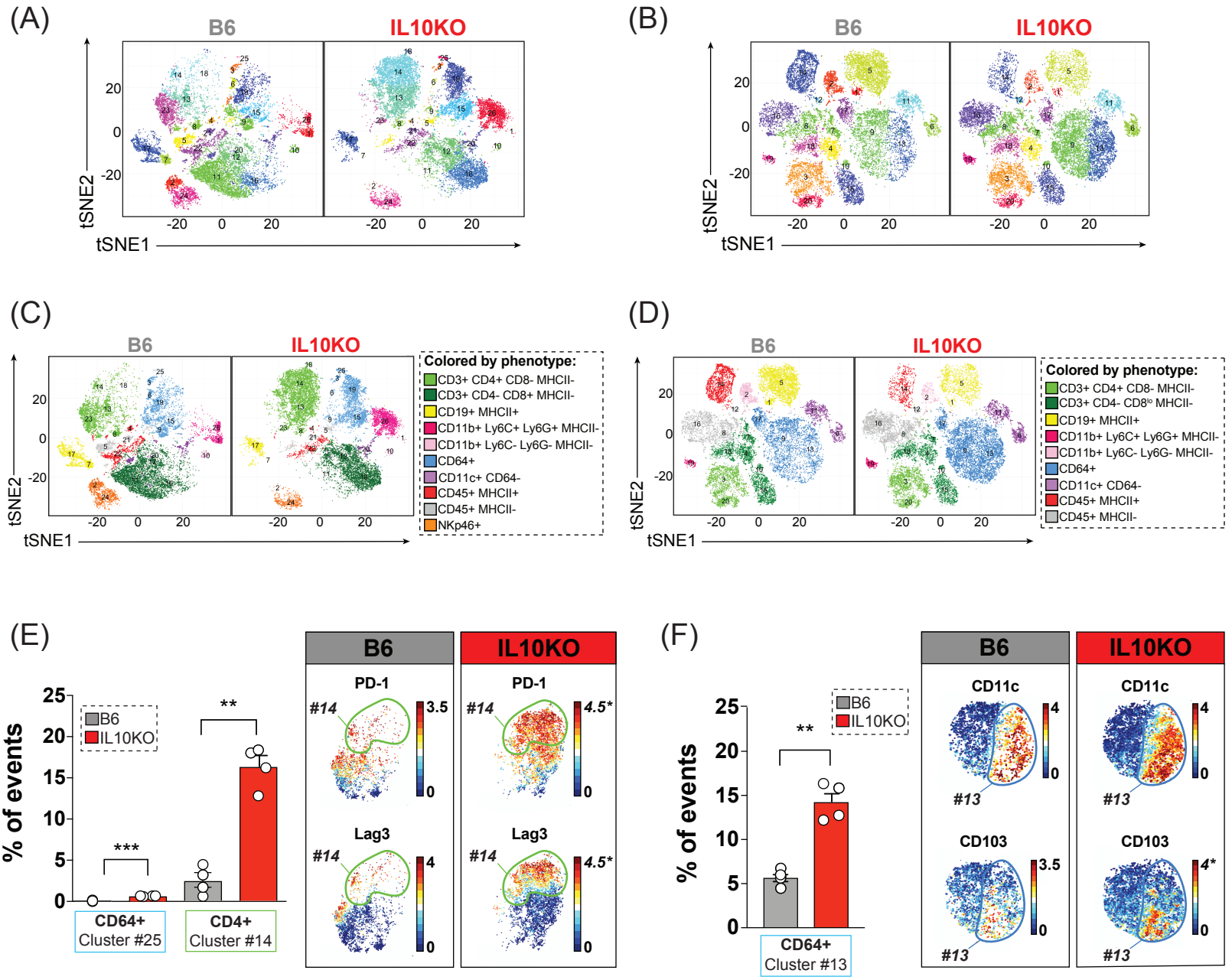

Kimball et al
Figure 4

CD4 T cells (191+ 193+ 195- CD3+ CD4+ MHCII- events), stimulated for ICCS

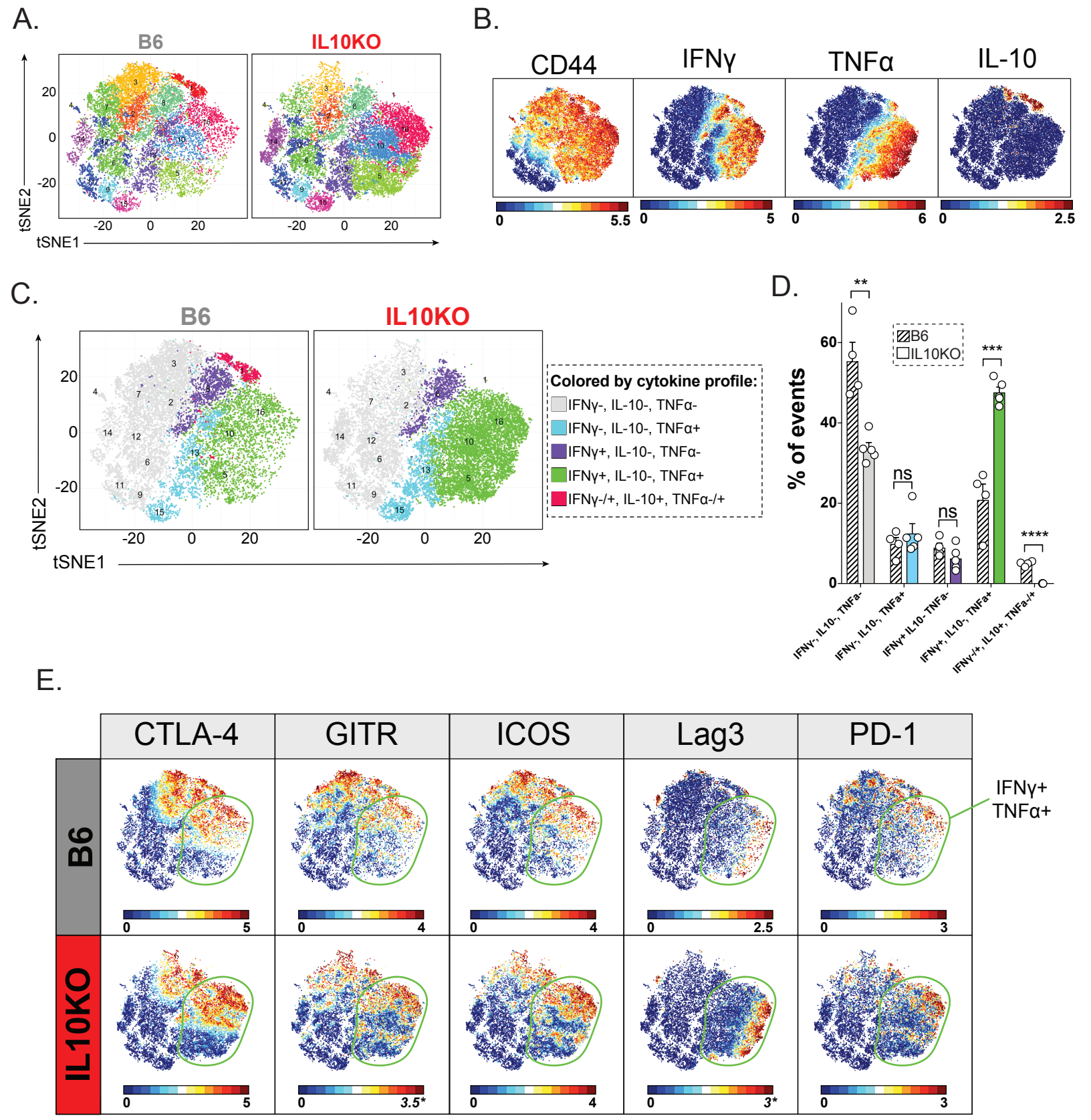

Kimball et al
Figure 5

Table 1. Antibody conjugates used for the analysis in Figure 1 and 5.

Tag	Target	Ab Clone	Surface/Intracellular	Clustering*
^{89}Y	CD45	30-F11	Surface	Yes
^{141}Pr	Gr1 (Ly6C/Ly6G)	RB6-8C5	Surface	Yes
^{142}Nd	CD11c	N418	Surface	Yes
^{143}Nd	GITR (CD357)	DTA1	Surface	Yes
^{144}Nd	IL-2	JES6-5H4	Intracellular	Yes
^{145}Nd	CD69	H1.2F3	Surface	Yes
^{146}Nd	CD8α	53-6.7	Surface	Yes
^{148}Nd	CD11b	M1/70	Surface	Yes
^{149}Sm	CD19	6D5	Surface	Yes
^{150}Nd	CD25	3C7	Surface	Yes
^{151}Eu	CD64	X54-5/7.1	Surface	Yes
^{152}Sm	CD3ε	145-2C11	Surface	No
^{153}Eu	PD-L1 (CD274)	10F.9G2	Surface	Yes
^{154}Sm	CTLA4 (CD152)	UC10-4B9	Intracellular	Yes
^{155}Gd	IRF4	3E4	Intracellular	Yes
^{156}Gd	FoxP3-PE / anti-PE	FJK-16s (Thermo Fisher) / PE001 (anti-PE)	Intracellular/Secondary	Yes
^{158}Gd	IL-10	JES5-16E3	Intracellular	Yes
^{159}Tb	PD-1 (CD279)	RMP1-30	Surface	Yes
^{160}Gd	GMCSF-FITC / anti-FITC	MP1-22E9 (Pharmingen) / FIT-22 (anti-FITC)	Intracellular/Secondary	Yes
^{161}Dy	Tbet	4B10	Intracellular	Yes
^{162}Dy	TNFα	MP6-XT22	Intracellular	No (Fig. 1) Yes (Fig. 5)
^{163}Dy	Lag3-APC / anti-APC	C9B7W (Biolegend) / APC003 (anti-APC)	Surface/Secondary	Yes
^{164}Dy	IkBα	L35A5	Intracellular	Yes
^{165}Ho	IFNγ	XMG1.2	Intracellular	No (Fig. 1) Yes (Fig. 5)
^{166}Er	IL-4	11B11	Intracellular	Yes
^{167}Er	IL-6	MP5-20F3	Intracellular	Yes
^{168}Er	Ki-67	B56	Intracellular	Yes
^{169}Tm	Ly-6A/E (Sca-1)	D7	Surface	Yes
^{170}Er	NK1.1 (CD161)	PK136	Surface	Yes
^{171}Yb	CD44	IM7	Surface	Yes
^{172}Yb	CD4	RM4-5	Surface	No
^{173}Yb	CD117 (ckit)	2B8	Surface	Yes
^{174}Yb	MHC class II (IA/IE)	M5/114.15.2	Surface	No
^{175}Lu	CD127	A7R34	Surface	Yes
^{176}Yb	ICOS (CD278)	7E.17G9	Surface	Yes
^{195}Pt	Cisplatin	Cell-ID Cisplatin		No
^{191}Ir, ^{193}Ir	Intercalator	Cell-ID Intercalator-Ir		No
^{140}Ce ^{151}Eu ^{153}Eu ^{165}Ho ^{175}Lu	Normalization Beads			No

*Clustering parameters used for Figure 1 and 5 differed as indicated.

Table 2. Antibody conjugates used for the analysis in Figure 2.

Tag	Target	Ab Clone	Surface/Intracellular	Clustering*
^{89}Y	CD45	30-F11	Surface	Yes
^{141}Pr	Gr1 (Ly6C/Ly6G)	RB6-8C5	Surface	Yes
^{142}Nd	CD11c	N418	Surface	Yes
^{143}Nd	CD103-Biotin / anti-Biotin	2E7 (Biolegend) / 1D4C3 (anti-Biotin)	Surface	Yes
^{144}Nd	MHC class I	28-14-8	Surface	Yes
^{145}Nd	CD69	H1.2F3	Surface	Yes
^{146}Nd	CD8α	53-6.7	Surface	Yes
^{150}Nd	CD27	LG.3A10	Surface	Yes
^{151}Eu	CD25	3C7	Surface	Yes
^{152}Sm	CD3ε	145-2C11	Surface	Yes (A) / No (B-D)
^{154}Sm	CD11b	M1/70	Surface	Yes
^{156}Gd	CD49b-PE / anti-PE	HMa2 (Biolegend) / PE001 (anti-PE)	Surface/Secondary	Yes
^{159}Tb	PD-1 (CD279)	RMP1-30	Surface	Yes
^{160}Gd	KLRG1-FITC / anti-FITC	2FI (Thermo Fisher) / FIT-22 (anti-FITC)	Surface/Secondary	Yes
^{161}Dy	Tbet	4B10	Intracellular	Yes
^{162}Dy	Ly6C	HK1.4	Surface	Yes
^{163}Dy	Lag3-APC / anti-APC	C9B7W (Biolegend) / APC003 (anti-APC)	Surface/Secondary	Yes
^{164}Dy	IkBα	L35A5	Intracellular	Yes
^{166}Er	CD19	6D5	Surface	Yes
^{167}Er	CD150	TC15-12F12.2	Surface	Yes
^{168}Er	Ki-67	B56	Intracellular	Yes
^{169}Tm	IL10gfp	5F12.4 (anti-GFP)	Intracellular	Yes
^{170}Er	CD40L	MR1	Surface	Yes
^{171}Yb	CD44	IM7	Surface	Yes
^{172}Yb	CD4	RM4-5	Surface	Yes (A) / No (B-D)
^{173}Yb	CD117 (ckit)	2B8	Surface	Yes
^{174}Yb	MHC class II (IA/IE)	M5/114.15.2	Surface	Yes (A) / No (B-D)
^{175}Lu	CD127	A7R34	Surface	Yes
^{176}Yb	ICOS (CD278)	7E.17G9	Surface	Yes
^{195}Pt	Cisplatin	Cell-ID Cisplatin		No
^{191}Ir, ^{193}Ir	Intercalator	Cell-ID Intercalator-Ir		No
^{140}Ce ^{151}Eu ^{153}Eu ^{165}Ho ^{175}Lu	Normalization Beads			No

*Clustering parameters used for Figure 2B-D excluded CD3ε, CD4, and MHC class II.

Table 3. Antibody conjugates used for the analysis in Figure 3.

Tag	Target	Ab Clone	Surface/Intracellular	Clustering
^{89}Y	CD45	30-F11	Surface	Yes
^{141}Pr	pSHP2 [Y580]	D66F10	Intracellular	Yes
^{142}Nd	CD11c	N418	Surface	Yes
^{143}Nd	GITR (CD357)	DTA1	Surface	Yes
^{144}Nd	CXCR3-FITC / anti-FITC	CXCR3-173 (Biolegend)/ FIT-22 (anti-FITC)	Surface/Secondary	Yes
^{145}Nd	CD69	H1.2F3	Surface	Yes
^{146}Nd	CD8α	53-6.7	Surface	Yes
^{147}Sm	pHistone H2A.X (SER139)	JBW301	Intracellular	Yes
^{148}Nd	CD11b	M1/70	Surface	Yes
^{149}Sm	CD19	6D5	Surface	Yes
^{150}Nd	CD27	LG.3A10	Surface	Yes
^{151}Eu	CD25	3C7	Surface	Yes
^{152}Sm	CD3ε	145-2C11	Surface	No
^{153}Eu	PD-L1 (CD274)	10F.9G2	Surface	Yes
^{154}Sm	CTLA4 (CD152)	UC10-4B9	Intracellular	Yes
^{155}Gd	IRF4	3E4	Intracellular	Yes
^{156}Gd	41BB-PE / anti-PE	17B5 (Thermo Fisher) / PE001 (anti-PE)	Surface/Secondary	Yes
^{158}Gd	FoxP3	FJK-16s	Intracellular	Yes
^{159}Tb	PD-1 (CD279)	RMP1-30	Surface	Yes
^{160}Gd	CD5	53-7.3	Surface	Yes
^{161}Dy	Tbet	4B10	Intracellular	Yes
^{162}Dy	Tim3 (CD366)	RMT3-23	Surface	Yes
^{163}Dy	BCL6	K112-91	Intracellular	Yes
^{164}Dy	IkBα	L35A5	Intracellular	Yes
^{165}Ho	Beta-catenin (active)	D13A1	Intracellular	Yes
^{166}Er	Arginase-1	Polyclonal	Intracellular	Yes
^{167}Er	Gata3	TWAJ	Intracellular	Yes
^{168}Er	Ki-67	B56	Intracellular	Yes
^{169}Tm	IL10gfp	5F12.4 (anti-GFP)	Intracellular	Yes
^{170}Er	CD49b	HMa2	Surface	Yes
^{171}Yb	CD44	IM7	Surface	Yes
^{172}Yb	CD4	RM4-5	Surface	No
^{173}Yb	CD117 (ckit)	2B8	Surface	Yes
^{174}Yb	Lag3 (CD223)	C9B7W	Surface	Yes
^{175}Lu	CD127	A7R34	Surface	Yes
^{176}Yb	ICOS (CD278)	7E.17G9	Surface	Yes
^{209}Bi	MHC class II (IA/IE)	M5/114.15.2	Surface	No
^{195}Pt	Cisplatin	Cell-ID Cisplatin		No
^{191}Ir, ^{193}Ir	Intercalator	Cell-ID Intercalator-Ir		No
^{140}Ce ^{151}Eu ^{153}Eu ^{165}Ho ^{175}Lu	Normalization Beads			No

Table 4A. Antibody conjugates used for the analysis in the lung (Figures 4A, 4C, and 4E).

Tag	Target	Ab Clone	Surface/Intracellular	Clustering
^{89}Y	CD45	30-F11	Surface	No
^{141}Pr	Gr-1 (Ly6C/Ly6G)	RB6-8C5	Surface	Yes
^{142}Nd	CD11c	N418	Surface	Yes
^{143}Nd	GITR (CD357)	DTA1	Surface	Yes
^{144}Nd	MHC class I	28-14-8	Surface	Yes
^{145}Nd	CD69	H1.2F3	Surface	Yes
^{146}Nd	CD8α	53-6.7	Surface	Yes
^{148}Nd	CD11b	M1/70	Surface	Yes
^{149}Sm	p4E-BP1 [T37/T46]	236B4	Intracellular	Yes
^{150}Nd	CD25	3C7	Surface	Yes
^{151}Eu	CD64	X54-5/7.1	Surface	Yes
^{152}Sm	CD3ε	145-2C11	Surface	Yes
^{153}Eu	PD-L1 (CD274)	10F.9G2	Surface	Yes
^{154}Sm	CTLA4 (CD152)	UC10-4B9	Intracellular	Yes
^{155}Gd	IRF4	3E4	Intracellular	Yes
^{156}Gd	Siglec-F-PE / anti-PE	E50-2440 (BD Pharmingen) / PE001 (anti-PE)	Surface/Secondary	Yes
^{158}Gd	FoxP3	FJK-16s	Intracellular	Yes
^{159}Tb	PD-1 (CD279)	RMP1-30	Surface	Yes
^{160}Gd	KLRG1-FITC / anti-FITC	2FI (Thermo Fisher) / FIT-22 (anti-FITC)	Surface/Secondary	Yes
^{161}Dy	Tbet	4B10	Intracellular	Yes
^{162}Dy	Tim3 (CD366)	RMT3-23	Surface	Yes
^{163}Dy	Lag3-APC / anti-APC	C9B7W (Biolegend) / APC003 (anti-APC)	Surface/Secondary	Yes
^{164}Dy	IkBα	L35A5	Intracellular	Yes
^{165}Ho	Beta-catenin (active)	D13A1	Intracellular	Yes
^{166}Er	CD19	6D5	Surface	Yes
^{167}Er	NKp46	29A1.4	Surface	Yes
^{168}Er	Ki-67	B56	Intracellular	Yes
^{169}Tm	Ly-6A/E (Sca-1)	D7	Surface	Yes
^{170}Er	PD-L2-Biotin / anti-Biotin	TY25 (Biolegend) / 1D4-C5 (anti-Biotin)	Surface/Secondary	Yes
^{171}Yb	CD44	IM7	Surface	Yes
^{172}Yb	CD4	RM4-5	Surface	Yes
^{173}Yb	CD117 (ckit)	2B8	Surface	Yes
^{174}Yb	MHC class II (IA/IE)	M5/114.15.2	Surface	Yes
^{175}Lu	CD127	A7R34	Surface	Yes
^{176}Yb	ICOS	7E.17G9	Surface	Yes
^{195}Pt	Cisplatin	Cell-ID Cisplatin		No
^{191}Ir, ^{193}Ir	Intercalator	Cell-ID Intercalator-Ir		No
^{140}Ce ^{151}Eu ^{153}Eu ^{165}Ho ^{175}Lu	Normalization Beads			No

Table 4B. Antibody conjugates used for the analysis in the colon (Figures 4B, 4D, and 4F).

Tag	Target	Ab Clone	Surface/Intracellular	Clustering
^{89}Y	CD45	30-F11	Surface	No
^{141}Pr	Ly6G	1A8	Surface	Yes
^{142}Nd	CD11c	N418	Surface	Yes
^{143}Nd	CD103-Biotin / anti-Biotin	2E7 (Biolegend) / 1D4C3 (anti-Biotin)	Surface/Secondary	Yes
^{144}Nd	MHC class I	28-14-8	Surface	Yes
^{145}Nd	SiglecF-PE / anti-PE	E50-2440 (BD Pharmingen) / PE001 (anti-PE)	Surface/Secondary	Yes
^{146}Nd	CD8α	53-6.7	Surface	Yes
^{148}Nd	CD11b	M1/70	Surface	Yes
^{149}Sm	CD19	6D5	Surface	Yes
^{150}Nd	CD25	3C7	Surface	Yes
^{151}Eu	CD64	X54-5/7.1	Surface	Yes
^{152}Sm	CD3ε	145-2C11	Surface	Yes
^{153}Eu	PD-L1 (CD274)	10F.9G2	Surface	Yes
^{154}Sm	CTLA4 (CD152)	UC10-4B9	Intracellular	Yes
^{155}Gd	IRF4	3E4	Intracellular	Yes
^{156}Gd	CD90.2	30-H12	Surface	Yes
^{158}Gd	FoxP3	FJK-16s	Intracellular	Yes
^{159}Tb	RORgt	B2D	Intracellular	Yes
^{160}Gd	CXCR3-FITC / anti-FITC	CXCR3-173 (Biolegend) / FIT-22 (anti-FITC)	Surface/Secondary	Yes
^{161}Dy	Tbet	4B10	Intracellular	Yes
^{162}Dy	Ly6C	HK1.4	Surface	Yes
^{163}Dy	F4/80-APC / anti-APC	MB8 (Thermo Fisher) / APC003 (anti-APC)	Surface/Secondary	Yes
^{164}Dy	IkBα	L35A5	Intracellular	Yes
^{165}Ho	Beta-catenin (active)	D13A1	Intracellular	Yes
^{166}Er	Arginase-1	Polyclonal	Intracellular	Yes
^{167}Er	NKp46	29A1.4	Surface	Yes
^{168}Er	Ki-67	B56	Intracellular	Yes
^{169}Tm	Ly-6A/E (Sca-1)	D7	Surface	Yes
^{170}Er	CD49b	HMa2	Surface	Yes
^{171}Yb	CD44	IM7	Surface	Yes
^{172}Yb	CD4	RM4-5	Surface	Yes
^{173}Yb	CD117 (ckit)	2B8	Surface	Yes
^{174}Yb	Lag3 (CD223)	C9B7W	Surface	Yes
^{175}Lu	CD127	A7R34	Surface	Yes
^{176}Yb	ICOS (CD278)	7E.17G9	Surface	Yes
^{209}Bi	MHC class II (IA/IE)	M5/114.15.2	Surface	Yes
^{195}Pt	Cisplatin	Cell-ID Cisplatin		No
^{191}Ir, ^{193}Ir	Intercalator	Cell-ID Intercalator-Ir		No
^{140}Ce ^{151}Eu ^{153}Eu ^{165}Ho ^{175}Lu	Normalization Beads			No